HYDROGEN RECOMBINATION LINES NEAR 327 MHz. I. DISTRIBUTION OF LOW-DENSITY IONIZED GAS IN THE GALACTIC DISK

D. ANISH ROSHI

National Centre for Radio Astrophysics, Tata Institute of Fundamental Research, Pune, India

AND

K. R. ANANTHARAMAIAH

Raman Research Institute, Bangalore, India and National Radio Astronomy Observatory,[1] Socorro, New Mexico

ABSTRACT

We present the results of a low-resolution ($2° \times 2°$) survey of radio recombination lines (RRLs) near 327 MHz in the Galactic plane made with the Ooty Radio Telescope (ORT). Although the angular resolution is coarse, these observations represent the first contiguous survey of low-frequency RRL emission in the longitude range $l = 330°$–$0°$–$89°$ (inner Galaxy). Hydrogen RRLs were detected in almost all directions in the inner Galaxy and carbon lines in several positions. In the outer Galaxy ($l = 172°$–$252°$), an unbiased set of 14 positions were observed and lines were detected toward three of them. To study the extent of the ionized gas above the Galactic disk, we have observed RRLs along the Galactic latitude at two specific longitudes ($l = 0°.0$ and $13°.9$). RRLs were detected up to $b = \pm3°$. The l-v diagram and the radial distribution, obtained from RRL emission near 327 MHz, show good similarity with that of RRL emission near 1.4 GHz, "intense" ^{12}CO emission and to some extent with the RRLs observed near 3 cm from normal H II region. These distributions are distinctly different from those of Hα and H I emission from the Galactic disk. Based on a comparison of the radial distribution of different components in the Galactic disk, we conclude that the diffuse RRL emission is associated with star-forming regions and possibly with a low-density component of known H II regions in the inner Galaxy.

Subject headings: diffuse radiation — H II regions — ISM: molecules — ISM: structure — radio lines: ISM

1. INTRODUCTION

Radio recombination lines (RRLs) are an useful tool for studying the properties of different types of ionized gas in the Galaxy. The Galactic plane contains several forms of ionized gas. At one extreme there are the two types of widely distributed ionized gases of very low average density which are a part of the general interstellar medium: the warm ionized medium (WIM) with $T_e \sim 10^4$ K and $\langle n_e \rangle \sim 0.03$ cm^{-3}; and the hot ionized medium (HIM) or the coronal gas with $T_e \sim 10^6$ K and $\langle n_e \rangle \sim 0.003$ cm^{-3} (McKee & Ostriker 1977; Kulkarni & Heiles 1988). The volume-filling factor of these components in the ISM is large ($f \sim 0.2$–0.7). At the other extreme are the ultracompact H II regions with $n_e > 10^4$ cm^{-3} and sizes $\ll 1$ pc, which are formed around young, hot stars (Wood & Churchwell 1989). Between these two extremes, there are a variety of H II regions over a wide range of densities ($n_e \sim 1$–1000 cm^{-3}) and a relatively narrow range of temperatures ($T_e \sim 3000$–$10,000$ K). The sizes of these regions range from a few parsecs to few tens of parsecs. Somewhere between the two extremes mentioned above, there also appears to be a low-density extended ionized component in the inner Galaxy. This component has been referred to as "extended low-density" (ELD) ionized gas by Mezger (1978) and as "extended low-density warm ionized medium" (ELDWIM) by Petuchowski & Bennett (1993), Heiles (1994), and Heiles, Reach, & Koo (1996).

Observationally, the low-density extended ionized medium in the inner Galaxy was identified through the detection of radio recombination lines at several positions along the Galactic plane which are free of discrete continuum sources (Gottesman & Gordon 1970; Gordon & Cato 1972). Subsequently, this low-density component has been systematically observed in radio recombination lines near 1.4 GHz by Hart & Pedlar (1976), Lockman (1976, 1980), Cersosimo (1990), and Heiles et al. (1996). Recombination lines from this gas was also observed by Anantharamaiah (1985a, 1985b) near 325 MHz. This paper is concerned with new extensive observations of this low-density ionized component in radio recombination lines at frequencies near 327 MHz using the Ooty Radio Telescope (ORT).

From the theory of RRL, it can be shown that recombination lines at low frequencies (< 1 GHz) do not originate in normal high-density H II regions because of the effects of continuum opacity, pressure broadening and beam dilution (Shaver 1975). Observations of low-frequency RRLs are therefore sensitive to relatively low-density ($0.5 < n_e < 50$ cm^{-3}), large angular size (tens of arcminutes) ionized regions. At the current sensitivities, low-density ionized gas in the Galactic plane with emission measures greater than a few hundred cm^{-6} pc is detectable in radio recombination lines at low frequencies. Low-frequency RRLs are thus not sensitive enough to detect the WIM, which typically has emission measures of 4–6 cm^{-6} pc for a path length of 1 kpc through the Galactic plane. In contrast, the Hα line in the optical band can be detected from the WIM at least within 1–2 kpc from the Sun (Reynolds 1990 and references therein) in directions toward which interstellar extinction is low.

The detection of low-frequency RRLs from almost all observed positions in the Galactic longitude range 0°–40°, has led to different suggestions for the origin of the low-density gas. For example, Mathews, Pedlar, & Davies (1973), Shaver (1976), and Mezger (1978) have suggested that they are large, evolved low-density H II regions. On the other hand, Anantharamaiah (1986) has argued that this low-density gas is simply the outer envelopes of the normal (usually higher density) H II regions. Based on the ubiquity of the RRL emission in the inner Galaxy as seen in their recent observations, Heiles, Reach, & Koo (1996) have associated the lines with the ELDWIM, which they picture as a higher density version of the local WIM. Heiles et al. (1996) also suggest that about 17% of the low-frequency emission arises in "wormlike" structures that are the walls of cavities blown by clustered supernova and ionized by hot stars in the same cluster.

To understand the extended low-density ionized gas in the inner Galaxy it is essential to determine the distribution of the gas in the Galactic plane and compare it with that of other components of the ISM. It is also essential to determine the physical properties of the ionized gas. A complete survey of the Galactic plane will help in determining the distribution and making the comparison. When combined with other observations, such a survey will also help in determining the physical properties of the gas. With these objectives in mind, we have performed a survey of RRLs near 327 MHz in the Galactic plane using the ORT. The angular resolution of the observations is $\sim 2° \times 2°$. Although the angular resolution is coarse, these observations represent the first contiguous survey of recombination line emission in the longitude range $l = 330°$–$0°$–$89°$.

In this paper, we present the observations and derive the distribution of the ionized gas in the Galactic disk and compare it with the distribution of other components. Deriving the physical properties using these and other existing observations will be the subject of another publication. This paper is organized as follows. The observations and data reduction are described in § 2, and the results are presented in § 3 . Section 4 discusses the distribution of the ionized gas in the Galactic plane using an l-v diagram and compute the radial distribution of the ionized gas. These distributions are compared with similar diagrams obtained from RRLs observed near 1.4 GHz, higher frequency RRLs from H II regions, Hα and ^{12}CO observations. The latitude extent of the ionized gas is also discussed in this section. Observations toward the outer Galaxy and their interpretation are presented in § 5. The results are summarized in § 6.

2. OBSERVATIONS AND DATA REDUCTION

The RRL survey was made using the ORT which is a 530 m × 30 m parabolic cylinder operating at a nominal center frequency of 327 MHz (Swarup et al. 1971). In the normal configuration of the ORT, the signals received by groups of 48 dipoles of the 1056 element linear array at the focal line are added in-phase. Twenty-two such groups, which are known as "modules," are combined later to produce a beam of $\sim 2° \times 5.5$ sec (δ), δ being the declination. The half power beam width of a single module is 2°3 (in R.A.) × 2°2 sec (δ) (in declination). The spectrometer used for the observations (see below) was configured to collect data from two such modules separately. The incoherent addition of the signals from the two modules preserves the spatial

resolution and under certain conditions increases the signal to noise ratio by $\sqrt{2}$.

The center frequency of operation of the telescope is 326.5 MHz. The RRL transitions from principal quantum numbers $n = 270, 271, 272, 273$, and $\Delta n = 1$ fall inside the 15.0 MHz bandwidth of the ORT. A new digital back end was built to simultaneously observe all four transitions with a velocity resolution of ~ 1.0 km s^{-1}. This back end utilizes an existing 512 channel one-bit autocorrelation spectrometer (Subrahmanyan 1989) to generate 6144 spectral channels using the technique of "recirculation". The system samples eight base-band signals of 768 kHz bandwidth at the Nyquist rate and measures the autocorrelation over 768 lags for each of them. The correlator gives a spectral resolution of 1 kHz for each base band. Using this system, four RRL transitions from two modules, which amount to eight independent spectra, were obtained simultaneously. The reference spectrum was obtained by switching the frequency every second by half the bandwidth (i.e., 384 kHz). This switching scheme shifts the expected spectral line alternately between the two halves of the 768 kHz observing band, thus maximizing the effective integration time. The velocity coverage is about 320 km s^{-1} after rejecting the edge channels. The autocorrelation functions corresponding to the two frequency settings were integrated separately for 1 minute in the data acquisition computer and then written into a file, which formed the raw data. The local oscillator frequency was adjusted for each observation such that the expected spectral line appeared at the "reference" channel.

The reduction of the raw data to obtain the final spectrum and the estimation of the observed line parameters involved several steps. The autocorrelation values were examined for each integration, and any bad correlation values were replaced by interpolated values from adjacent lags. The on-line and reference spectra were obtained by Fourier-transforming the autocorrelation values after applying a Hanning weighting function. The difference spectra were constructed for each integration and a cubic baseline was removed from the spectrum after excluding the channels where line emission is expected. Individual spectra were carefully examined for interference. Spectra that were badly affected by interference were discarded. Spectra which had narrowband interference in only a few channels were retained, but the channels that were affected by interference were given a weight of zero while averaging the spectra. The sum of weights for each channel was kept track of separately until the final spectrum was obtained. This method resulted in slightly different integration times for each channel. Typically, the maximum difference in integration time was less than 10%.

The eight final spectra, corresponding to the four transitions observed simultaneously in two modules, and the respective channel weights were then transferred to the UniPops single-dish spectral line analysis software package developed by the National Radio Astronomy Observatory (Salter, Maddalena, & Garwood 1994). Channels showing any residual interference were removed by setting their channel weights to zero. The two halves of each spectra were first averaged to get the "folded" spectrum. The eight "folded" spectra were then averaged to obtain the final spectrum. Small differences in the velocity resolution of the different spectra were ignored. Typical effective integration time for a final spectrum is ~ 20 hr. The final integrated

spectrum was convolved with a box function of appropriate width to improve the signal to noise ratio. In all positions where the lines were detected, the spectral features could be seen in the corresponding smoothed spectra. If a residual baseline was present in the smoothed spectrum, then a linear, quadratic or a cubic function was fitted to the spectral points outside the line channels and subtracted from the spectrum. The line parameters were then obtained by fitting a Gaussian profile. The programs in UniPops were modified to take into account the different channel weights while performing these operations on the spectrum.

Along with the spectral measurements, we also measured the system temperature and continuum antenna temperature toward the observed positions. For observations in the Galactic plane near 327 MHz the system temperature is dominated ($>60\%$) by the nonthermal background emission. The system temperature is required to convert the spectral estimate to units of antenna temperature. This conversion is required since the spectral estimates are obtained with a one-bit autocorrelation spectrometer, which gives a normalized spectrum. Since the ORT does not have a noise injection facility, we obtained the system temperature by measuring the increase in the antenna output power with respect to an off-source position. Using an estimate of the receiver temperature, the spill over contribution and the sky temperature at the off-source position, we derived the system temperature and continuum temperature from the measured increase in the antenna output power. The off-source sky temperature at 327 MHz was obtained from the 408 MHz all-sky continuum map (Haslam et al. 1982) after convolving it with a $2° \times 2°$ beam and scaling the value to 327 MHz using a spectral index of -2.7 for the Galactic background radiation. In a few positions where we did not make such continuum measurements, the values were estimated from the 408 MHz map after convolving the map with the appropriate beam and scaling the values to 327 MHz. We estimate that the error in the measured continuum temperature is $\sim 10\%$.

The observed positions can be broadly classified into three categories.

1. *The Inner Galaxy:* We refer to the longitude range $l = 332°–0°–89°$ as the inner Galaxy. In this longitude range we have conducted an unbiased contiguous sampling of the Galactic plane. A total of 51 spectra at $b = 0°$ and separated in longitude by $\sim 2° \times \sec(\delta)$, δ being the declination, were taken.

2. *The Outer Galaxy:* A total of 14 positions, equally spaced in longitude, were observed in the range $172° < l < 252°$. This longitude range was coarsely sampled since earlier observations had indicated that RRLs at a low-frequency are not widely detected in the outer Galaxy (Anantharamaiah 1985a).

3. *Scans along Galactic Latitude :* At two specific longitudes in the inner Galaxy ($l = 0°.0$ and $13°.9$), spectra were taken in steps of $1°$ up to $b = \pm 4°$ to study the latitude extent of the ionized gas.

3. RESULTS

The recombination line spectra observed in the inner Galaxy are shown in Figure 1a. The spectra from the outer galaxy are shown in Figure 1b. The spectra obtained at different latitudes are shown in Figures 1c and 1d. All the spectra are plotted in units of line-to-continuum temperature ratio (T_L/T_C) against the LSR (local standard of rest) velocity computed with respect to the rest frequency of the H272α transition. The spectra are smoothed to the velocity resolution given in the seventh column of Table 1. In many of the spectra, two emission features are detected. The feature at higher velocity is the hydrogen line and the feature which is about -150 km s^{-1} from the hydrogen line is most likely a carbon recombination line. All the line features detected in this survey are in emission.

Table 1 gives the line parameters derived from the spectra. 1 σ errors obtained from the Gaussian fit are also given along with the line parameters. On the average, the integration time for each position is ~ 20 hr and the RMS noise (in units of T_L/T_C) is typically 1.5×10^{-4}.

3.1. Hydrogen Line

RRLs of hydrogen were detected in $\sim 80\%$ of the observed positions in the inner Galaxy. On the other hand, only three out of the 14 observed positions yielded detection in the outer Galaxy. The observations along the Galactic latitude detected lines up to $b \sim \pm 3°$ (Figs. 1c and 1d). The line-to-continuum ratio of the hydrogen line ranges from 0.3×10^{-3} to 1.4×10^{-3}. These values are comparable to T_L/T_C observed near 327 MHz by Anantharamaiah (1985a, 1985b) using a beam of $2° \times 5°.5$. The lines in the longitude range $l = 50°–70°$ are detected for the first time.

3.1.1. Line Widths

Figure 2a shows the distribution of the observed width of the hydrogen line. The median is 31.3 km s^{-1}. These line widths are larger than the typical line widths observed from both "compact" (Downes et al. 1980; Caswell & Haynes 1987; Lockman 1989) and "diffuse" H II regions (~ 26 km s^{-1}) (Lockman, Pisano, & Howards 1996). Comparing the observed line widths with those found in earlier surveys at higher frequencies, we find that larger line widths (>30 km s^{-1}) are more frequent in the present observations. At 327 MHz, the line widths can be affected by pressure broadening if the densities are higher than 30 cm^{-3} (Shaver 1975). However, the estimated densities (D. A. Roshi & K. R. Anantharamaiah 2000, in preparation) are too low for this effect to be significant. It is possible that the large line widths are due to blending of lines at different central velocities within the $2° \times 2°$ beam. A few of the positions (e.g. G355.3+0.0) show narrow hydrogen lines (~ 14 km s^{-1}). Such narrow lines were earlier observed from some normal H II regions (Shaver, McGee, & Pottasch 1979; Lockman 1989; Lockman et al. 1996). Upper limit for the temperature of the ionized gas obtained from the width of these narrow lines is ~ 4300 K.

3.1.2. Stimulated Emission

Figure 3a shows a plot of the line antenna temperature near 327 MHz against the corresponding continuum antenna temperature at the observed positions. Since the continuum temperature at these frequencies is dominated by the Galactic nonthermal emission, the observed correlation (correlation coefficient = 0.88) implies stimulated emission. The line to continuum ratio at these frequencies is approximately the line optical depth. Since the line optical depth is a function of the physical properties of the ionized
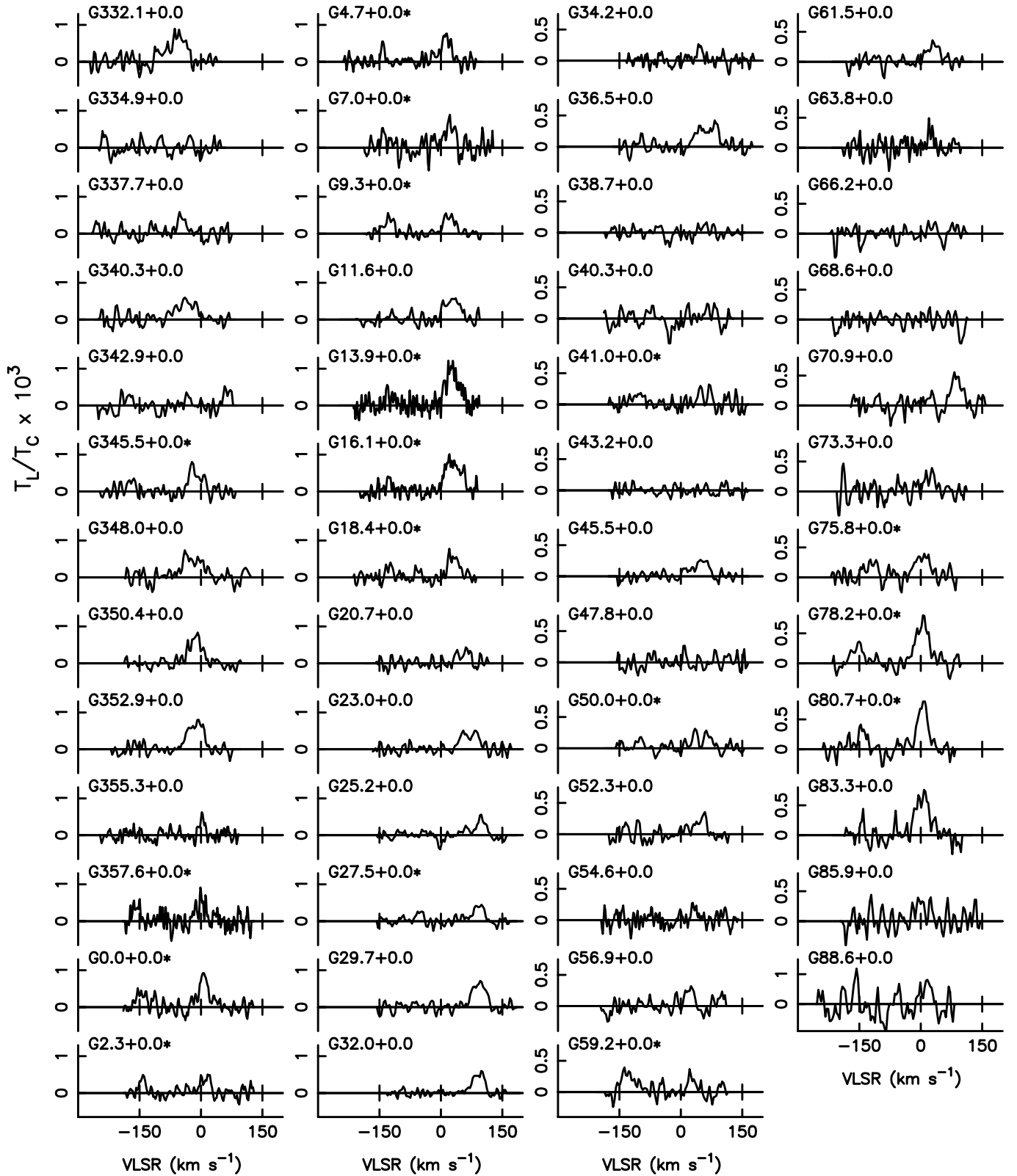
FIG. 1a

FIG. 1.—(a) Spectra of recombination lines near 327 MHz observed toward the inner Galaxy. The Galactic coordinates of the observed positions are indicated in each of the spectra. The ordinate is line to continuum ratio (T_L/T_C) and the abscissa is LSR velocity. The feature closer to 0 km s^{-1} is the hydrogen recombination line. In spectra indicated by asterisks along with the Galactic coordinates, the corresponding carbon recombination line as can be seen $-$ 150 km s^{-1} away. The ordinate scale of the spectra is different for columns 3 and 4. (b) Spectra of recombination lines near 327 MHz observed toward the outer Galaxy. The Galactic coordinates of the observed positions are indicated in each of the spectra. Possible hydrogen line near 0 km s^{-1} is present in only three of the observed spectra. (c) Observed spectra of recombination lines near 327 MHz as a function of Galactic latitude at $l = 0°.0$. The feature near 0 km s^{-1} is the hydrogen line and the feature near $-$ 150 km s^{-1} is the carbon line. (d) Observed spectra of hydrogen recombination lines near 327 MHz as a function of Galactic latitude at $l = 13°.9$. The ordinate is line to continuum ratio.
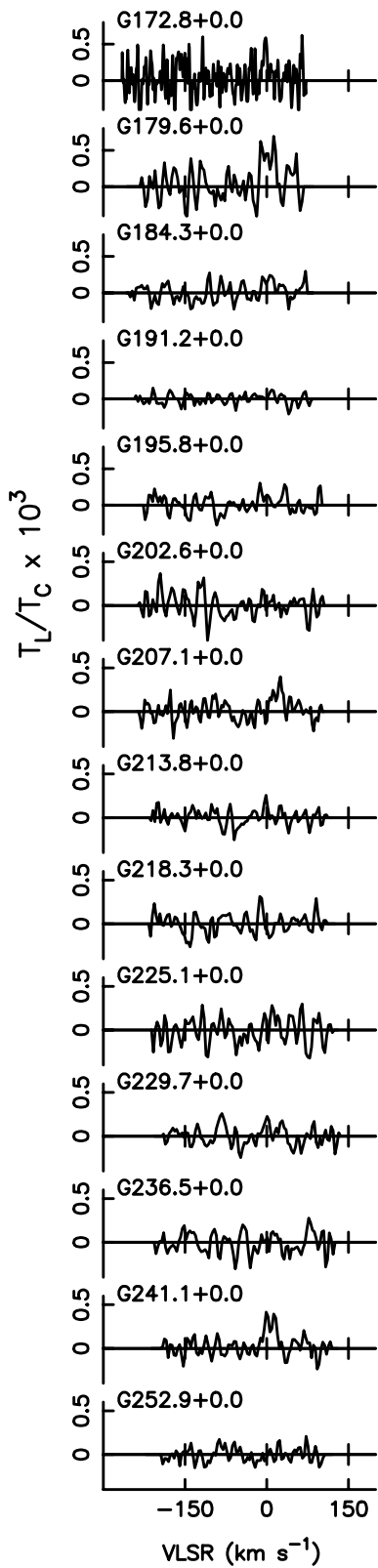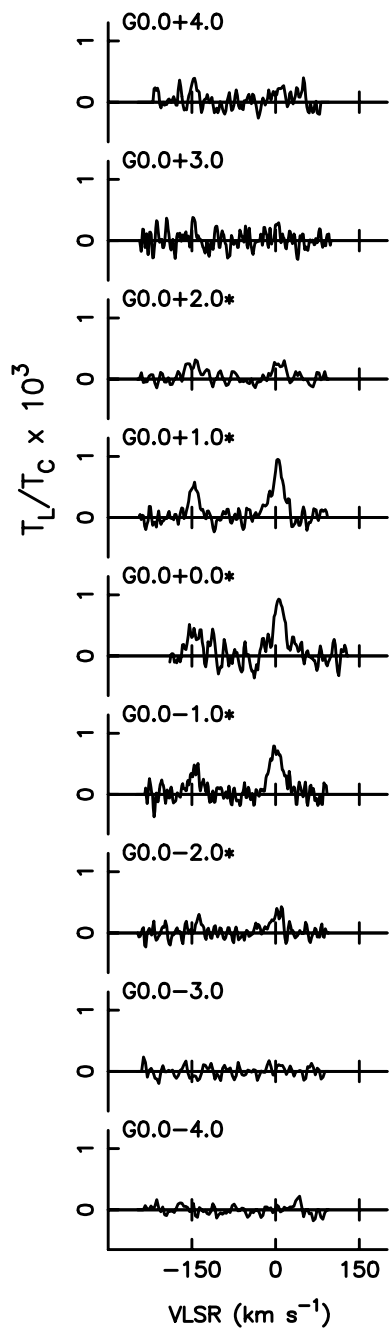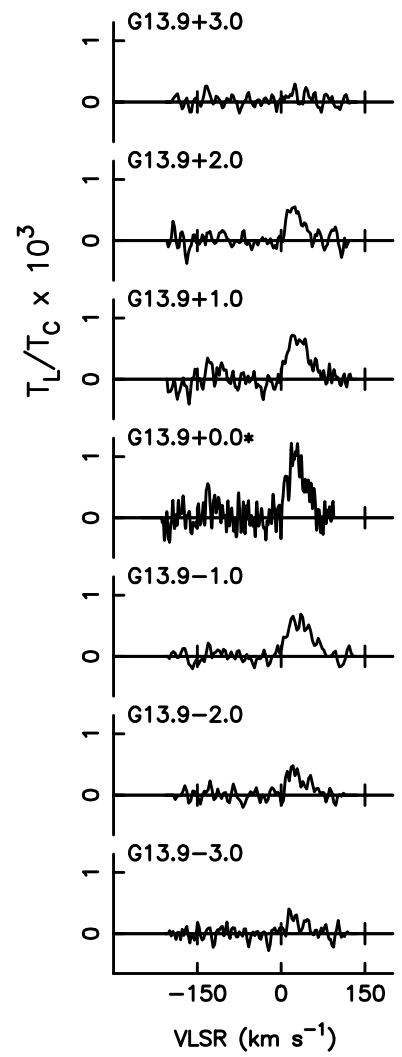
234

FIG. 1b

FIG. 1c

FIG. 1d

235

l(deg)	b (deg)	T_L/T_C ($\times 10^3$)	T_L (mK)	ΔV (km s^{-1})	$V_{\rm LSR}$ (km s^{-1})	$V_{\rm res}$ (km s^{-1})	RMS[a] ($\times 10^3$)	$t_{\rm int}$ (hr)	$T_C^{\rm b}$ (K)	Note
332.1......	+0.0	0.79(0.04)	133(7)	47.8(2.7)	-58.4(1.1)	8	0.22	7.6	257	h
334.9......	+0.0	...	...	...	...	8	0.21	9.9	259	
337.7......	+0.0	0.60(0.03)	133(6)	23.1(1.1)	-48.3(0.5)	8	0.17	9.1	341	h
340.3......	+0.0	0.59(0.02)	120(4)	54.1(2.4)	-36.3(1.0)	8	0.14	10.0	313	h
342.9......	+0.0	...	...	...	...	8	0.22	7.8	325	
345.5......	+0.0	0.78(0.04)	188(9)	34.2(1.8)	-16.0(0.8)	8	0.18	8.2	371	h
		0.42(0.05)	101(12)	19.2(2.6)	-170.9(1.1)					c
348.0......	+0.0	0.58(0.03)	148(7)	53.6(2.9)	-22.6(1.2)	8	0.19	12.7	395	h
350.4......	+0.0	0.89(0.03)	221(7)	35.3(1.4)	-14.0(0.6)	8	0.14	13.3	380	h
352.9......	+0.0	0.91(0.02)	288(7)	42.6(1.2)	-13.6(0.5)	8	0.14	11.9	490	h
355.3......	+0.0	0.64(0.05)	216(17)	13.4(1.2)	2.2(0.5)	5	0.16	17.0	519	h
357.6......	+0.0	0.63(0.05)	291(23)	26.2(2.4)	-1.2(1.0)	3	0.21	8.0	714	h
		0.47(0.05)	216(25)	22.2(3.0)	-158.7(1.3)					c
0.0	+0.0	0.94(0.04)	663(28)	29.0(1.4)	5.9(0.6)	5	0.17	11.4	1085	h
		0.42(0.04)	296(27)	29.2(3.1)	-146.8(1.3)					c
2.3	+0.0	0.46(0.03)	209(14)	26.0(2.0)	10.2(0.8)	6	0.13	10.7	699	h
		0.55(0.04)	247(17)	16.1(1.3)	-143.2(0.6)					c
4.7	+0.0	0.90(0.03)	379(13)	28.8(1.2)	11.3(0.5)	5	0.15	13.1	644	h
		0.76(0.06)	318(24)	8.5(0.7)	-142.6(0.3)					c
7.0	+0.0	0.78(0.06)	347(27)	24.8(2.2)	20.6(0.9)	5	0.25	7.2	685	h
		0.64(0.08)	283(37)	12.1(1.9)	-141.6(0.8)					c, t
9.3	+0.0	0.63(0.02)	255(10)	33.9(1.5)	19.6(0.6)	8	0.12	14.9	624	h
		0.49(0.03)	198(11)	23.5(1.5)	-126.7(0.6)					c
11.6	+0.0	0.70(0.02)	269(8)	43.0(1.5)	27.2(0.6)	8	0.14	12.6	591	h
13.9	+0.0	1.20(0.04)	513(18)	38.1(1.5)	26.9(0.6)	2	0.21	16.9	657	h
		0.74(0.11)	317(45)	6.0(1.0)	-131.8(0.4)					c, t
16.1	+0.0	1.02(0.03)	375(10)	46.6(1.4)	28.8(0.6)	3	0.15	16.8	568	h
		0.53(0.06)	197(21)	10.7(1.3)	-127.4(0.6)	...	...	...	...	c
18.4	+0.0	0.77(0.03)	299(13)	30.6(1.6)	30.0(0.7)	6	0.16	10.8	599	h
		0.36(0.05)	141(18)	17.3(2.5)	-125.5(1.1)	...	...	...	...	c
20.7	+0.0	0.40(0.03)	142(12)	34.2(3.4)	55.2(1.4)	8	0.17	11.6	540	h
23.0	+0.0	0.57(0.02)	217(9)	50.6(2.4)	70.2(1.0)	8	0.13	15.1	588	h
25.2	+0.0	0.61(0.03)	221(10)	26.0(1.4)	97.3(0.6)	8	0.13	19.9	554	h
27.5	+0.0	0.55(0.02)	183(8)	28.5(1.4)	91.6(0.6)	8	0.11	18.1	513	h
		0.39(0.03)	130(10)	16.9(1.5)	-52.6(0.6)	...	...	...	...	c
29.7	+0.0	0.88(0.02)	291(8)	36.2(1.1)	92.2(0.5)	8	0.13	17.7	510	h
32.0	+0.0	0.82(0.02)	227(7)	31.7(1.1)	91.2(0.5)	8	0.12	15.0	424	h
34.2	+0.0	0.34(0.02)	117(6)	14.2(0.9)	45.6(0.4)	5	0.10	38.4	524	h,t
36.5	+0.0	0.41(0.02)	107(4)	60.0(3.2)	65.2(1.2)	8	0.11	33.5	407	h
38.7	+0.0	...	...	...	...	8	0.11	27.6	392	
40.3	+0.0	...	...	...	...	8	0.18	21.8	361	
41.0	+0.0	0.26(0.02)	59(5)	36.3(3.8)	55.1(1.6)	8	0.12	20.7	348	h
		0.21(0.02)	47(5)	36.5(4.7)	-104.8(2.0)	...	...	...	...	c
43.2	+0.0	...	...	...	...	8	0.10	26.7	307	
45.5	+0.0	0.35(0.02)	60(3)	40.5(2.2)	48.8(0.9)	8	0.08	53.5	267	h
47.8	+0.0	...	...	...	...	8	0.15	26.1	267	
50.0	+0.0	0.30(0.02)	52(3)	58.3(4.3)	50.5(1.7)	8	0.11	45.3	268	h
		0.24(0.03)	42(6)	16.5(2.6)	-100.2(1.1)	...	...	...	...	c, t
52.3	+0.0	0.43(0.03)	54(3)	31.7(2.4)	49.6(1.0)	8	0.15	35.5	190	h
54.6	+0.0	0.42(0.03)	41(3)	14.2(1.3)	31.4(0.6)	5	0.17	48.5	150	h, t
56.9	+0.0	0.60(0.04)	45(3)	21.2(1.6)	20.9(0.7)	8	0.17	46.2	116	h
59.2	+0.0	0.55(0.04)	39(3)	21.0(2.0)	25.2(0.8)	8	0.16	22.3	109	h
		0.55(0.04)	39(2)	33.9(2.4)	-129.8(1.0)	...	...	...	...	c
61.5	+0.0	0.57(0.02)	38(2)	34.9(1.8)	29.4(0.8)	8	0.16	52.0	104	h
63.8	+0.0	0.66(0.06)	38(4)	14.7(1.6)	22.6(0.7)	5	0.26	39.4	88	h
66.2	+0.0	...	...	...	...	8	0.20	45.2	83	
68.6	+0.0	...	...	...	...	8	0.19	40.8	91	
70.9	+0.0	0.99(0.04)	65(3)	28.9(1.3)	86.2(0.6)	8	0.25	26.4	101	h, t
73.3	+0.0	0.54(0.04)	30(2)	29.1(2.3)	22.6(0.9)	6	0.21	47.1	86	h, t
75.8	+0.0	0.65(0.03)	45(2)	39.9(2.3)	3.4(1.0)	8	0.17	35.8	105	h
		0.39(0.04)	27(2)	33.5(3.4)	-121.5(1.5)	...	...	...	...	c
78.2	+0.0	1.05(0.02)	125(3)	35.1(1.0)	3.1(0.4)	8	0.13	26.9	183	h
		0.46(0.03)	55(3)	31.6(2.1)	-154.4(0.9)	...	...	...	...	c
80.7	+0.0	1.18(0.03)	142(4)	28.5(0.9)	4.1(0.4)	8	0.15	15.2	185	h

TABLE 1—*Continued*

l(deg)	b (deg)	T_L/T_C ($\times 10^3$)	T_L (mK)	ΔV (km s^{-1})	V_{LSR} (km s^{-1})	V_{res} (km s^{-1})	RMS[a] ($\times 10^3$)	t_{int} (hr)	T_C[b] (K)	Note
		0.53(0.04)	64(4)	21.3(1.7)	−143.9(0.7)	...	...	...	...	c
83.3	+0.0	1.03(0.04)	75(3)	37.8(1.6)	3.8(0.7)	8	0.22	13.0	113	h
85.9	+0.0	...	...	...	...	8	0.35	21.4	66	
88.6	+0.0	...	...	...	...	8	1.03	13.2	28	
					Outer Galaxy					
172.8	+0.0	...	...	...	...	2	0.54	26.9	58	
179.6	+0.0	1.48(0.20)	16(2)	24.4(3.8)	2.6(1.6)	8	0.66	46.4	17	h
184.3	+0.0	...	...	...	...	8	0.37	29.8	53	b
191.2	+0.0	...	...	...	...	8	0.20	36.5	75	
195.8	+0.0	...	...	...	...	8	0.32	30.6	70	
202.6	+0.0	...	...	...	...	8	0.37	20.3	61	
207.1	+0.0	0.87(0.07)	45(4)	21.7(2.1)	20.1(0.9)	6	0.31	23.3	80	h
213.8	+0.0	...	...	...	...	8	0.29	23.1	65	
218.3	+0.0	...	...	...	...	8	0.38	27.4	55	b
225.1	+0.0	...	...	...	...	8	0.52	11.4	55	b
229.7	+0.0	...	...	...	...	8	0.37	31.9	56	b
236.5	+0.0	...	...	...	...	8	0.41	18.4	55	b
241.1	+0.0	1.22(0.08)	43(3)	24.5(1.9)	6.0(0.8)	8	0.33	22.0	54	h
252.9	+0.0	...	...	...	...	8	0.29	27.5	55	
				Observations along Galactic Latitude						
0.0	−4.0	...	...	...	...	8	0.11	21.1	278	
0.0	−3.0	...	...	...	...	8	0.12	18.2	373	
0.0	−2.0	0.43(0.02)	164(10)	22.1(1.6)	2.2(0.7)	5	0.11	24.8	593	h
...	...	0.35(0.04)	135(15)	10.0(1.3)	−138.0(0.5)	...	...	...	...	c
0.0	−1.0	0.82(0.02)	530(14)	28.9(0.9)	0.5(0.4)	3	0.10	25.1	998	h
...	...	0.45(0.02)	291(15)	25.4(1.5)	−145.0(0.6)	...	...	...	...	c
0.0	+1.0	0.96(0.02)	449(12)	24.9(0.8)	3.4(0.3)	5	0.10	23.7	721	h
...	...	0.61(0.03)	287(13)	19.6(1.0)	−146.9(0.4)	...	...	...	...	c
0.0	+2.0	0.35(0.02)	108(7)	23.3(1.7)	5.2(0.7)	8	0.09	23.2	482	h
...	...	0.32(0.02)	99(6)	33.7(2.2)	−148.6(0.9)	...	...	...	...	c
0.0	+3.0	...	...	...	...	3	0.19	27.2	344	
0.0	+4.0	...	...	...	...	5	0.18	25.1	254	
13.9	−3.0	0.34(0.03)	71(5)	42.0(4.0)	23.4(1.6)	6	0.15	16.9	207	h
13.9	−2.0	0.47(0.03)	125(8)	40.1(3.1)	27.4(1.3)	8	0.14	20.0	269	h
13.9	−1.0	0.72(0.02)	275(7)	49.5(1.4)	31.1(0.6)	8	0.11	21.1	384	h
13.9	+1.0	1.01(0.02)	361(8)	48.8(1.2)	30.4(0.5)	5	0.16	21.3	358	h
13.9	+2.0	0.74(0.02)	193(6)	30.9(1.1)	23.2(0.5)	6	0.12	19.7	260	h
13.9	+3.0	...	...	...	...	6	0.14	20.8	207	

NOTE—h denotes hydrogen line, c denotes carbon line, t for tentative detection, b for blank region.
[a] RMS is in units of T_L/T_C
[b] Continuum temperature is the measured antenna temperature divided by 0.65, which is the beam efficiency factor. The error in these measurements are ~10%.

gas producing the line (Shaver 1975), the scatter of the data points in Figure 3a can be partly due to different physical properties of ionized gas in different directions. Another effect which can also contribute to this scatter is the different distances to the ionized gas, which changes the foreground contribution to the continuum temperature. Nevertheless, Figure 3a is a clear indication of the dominance of stimulated emission. The importance of stimulated emission of RRLs at low frequencies was discussed earlier by Shaver (1975). It was observed toward the Galactic center region by Pedlar et al. (1978) and Roshi & Anantharamaiah (1997) and in the Galactic plane by Anantharamaiah (1985a).

3.2. Carbon Line

The emission feature seen at about −150 km s^{-1} with respect to the hydrogen line in several spectra in Figures

1a–1d is most likely due to carbon. The line to continuum ratio of the carbon line ranges from 0.3×10^{-3} to 1.7×10^{-3}. The line to continuum ratio at some of the positions are comparable to or even more than that of the hydrogen line. The distribution of the width of the observed carbon lines are shown in Figure 2b. Widths of the carbon lines vary over a wide range; 6.0–37 km s^{-1}. A plot of the carbon line intensity against the continuum emission at the corresponding position (Fig. 3b) shows good correlation (correlation coefficient = 0.88), indicating the presence of stimulated emission.

The carbon line is almost as strong as the hydrogen line in spite of the small C/H abundance ratio in the ISM ($<3 \times 10^{-4}$) indicates that the two lines arise in regions with different physical properties. The carbon lines seen in Figures 1a–1d most likely belong to the class of low-frequency recombination lines first observed in absorption
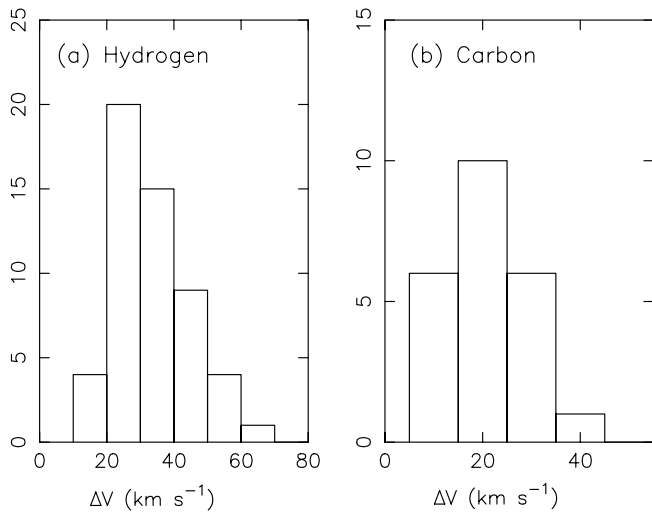
FIG. 2.—Histogram of the observed widths of (*a*) hydrogen, and (*b*) carbon recombination lines near 327 MHz in the Galactic plane.

at 26 MHz by Konovalenko & Sodin (1980). These RRLs were shown to turn over into emission above 200 MHz (Payne, Anantharamaiah, & Erickson 1989) and to be widespread in the inner Galaxy (Erickson, McConnell, & Anantharamaiah 1995; N. G. Kantharia & K. R. Anantharamaiah 2000, in preparation). We defer further discussion of the carbon lines from this survey to a future publication.

4. DISTRIBUTION OF THE IONIZED GAS IN THE GALACTIC DISK

4.1. *Integrated Line Intensity versus Galactic Longitude*

The velocity-integrated line intensity of RRL emission and continuum intensity, both obtained with a beam of $\sim 2° \times 2°$ at 327 MHz, are plotted as a function of longitude in Figure 4. While the continuum intensity shows a
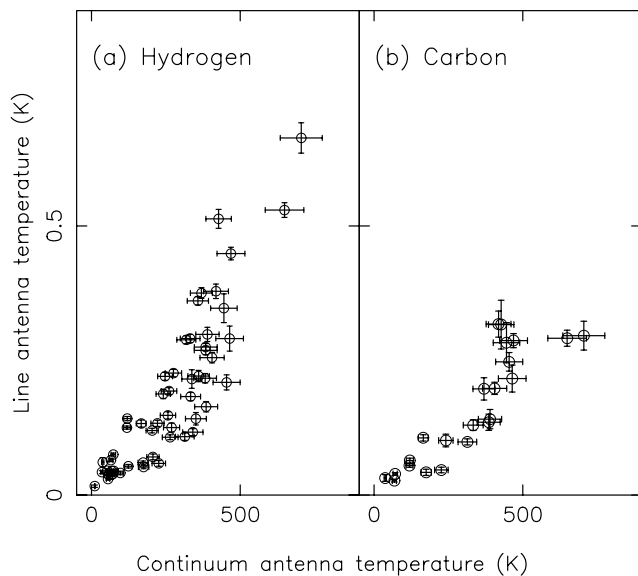
FIG. 3.—Antenna temperature of recombination lines near 327 MHz observed at different positions along the Galactic plane plotted against the measured continuum antenna temperature at the corresponding positions: (*a*) hydrogen (*b*) carbon.
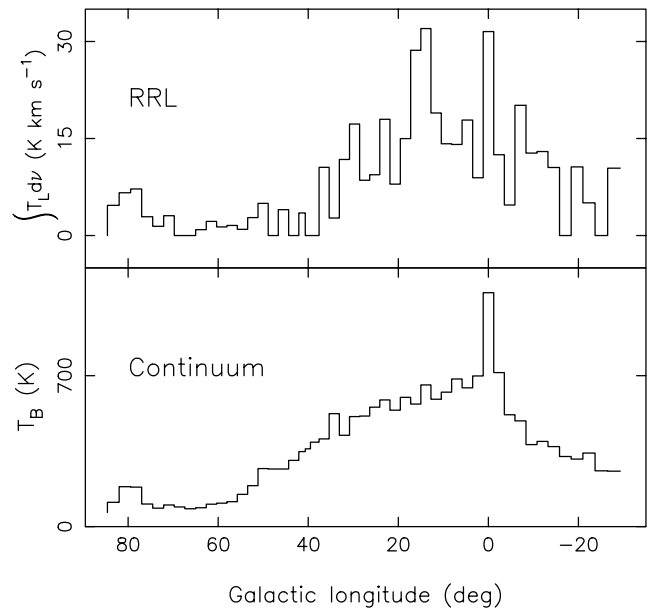
FIG. 4.—Velocity-integrated intensity of the hydrogen recombination line (*top*) and the continuum brightness temperature (*bottom*) near 327 MHz as a function of Galactic longitude in the inner Galaxy.

smooth variation with longitude, the line emission shows large fluctuations. These fluctuations imply that the line emitting region is not a uniform homogeneous medium, even after smoothing over $2°$. The prominent peaks in RRL emission are at longitudes $l = 0°$ and $l \sim 15°$. The enhanced line and continuum emissions near $l = 80°$ are associated with the well-known Cygnus complex.

4.2. *l-v Diagram*

The longitude-velocity diagram constructed from RRL observations of the Galactic plane can be used to understand the distribution of the ionized gas in the Galactic disk if we make the standard assumption that the observed central velocity of the line is due to differential galactic rotation. Figure 5*a* shows the *l-v* diagram obtained from the present data. For comparison (which is made below) we show in Figures 5*b*–5*e*, the *l-v* diagram obtained from other published spectral data. In all the frames in Figure 5, the expected *l-v* curves for gas located at Galactocentric radii 3.5 and 7 kpc are shown as dashed and dotted lines respectively. To obtain these curves and for subsequent work presented in this paper, we have used the parameters of galactic rotation given by Burton (1988) and by Burton & Gordon (1978). These parameters are scaled to conform with the most recent IAU-recommended Galactocentric distance of the Sun, $R_\odot = 8.5$ kpc, and circular velocity at Sun, $\theta_0 = 220$ km s^{-1}(Kerr & Lynden-Bell 1986). Figure 5*a* shows that most of the line emission originate from Galactocentric distances beyond 3.5 kpc. The line emission at longitudes less than $50°$ shows some confinement to the spiral arms 2 and 3. There does not seem to be much emission associated with arm 1. There is no line emission detected from the spiral arm 4 in the longitude range $20°$–$89°$. The central velocities of the lines detected at $l > 50°$ are close to the terminal velocities at these longitudes (see Fig. 5*a*). The large path-lengths with small velocity dispersion encountered at the tangent points probably helped in detecting
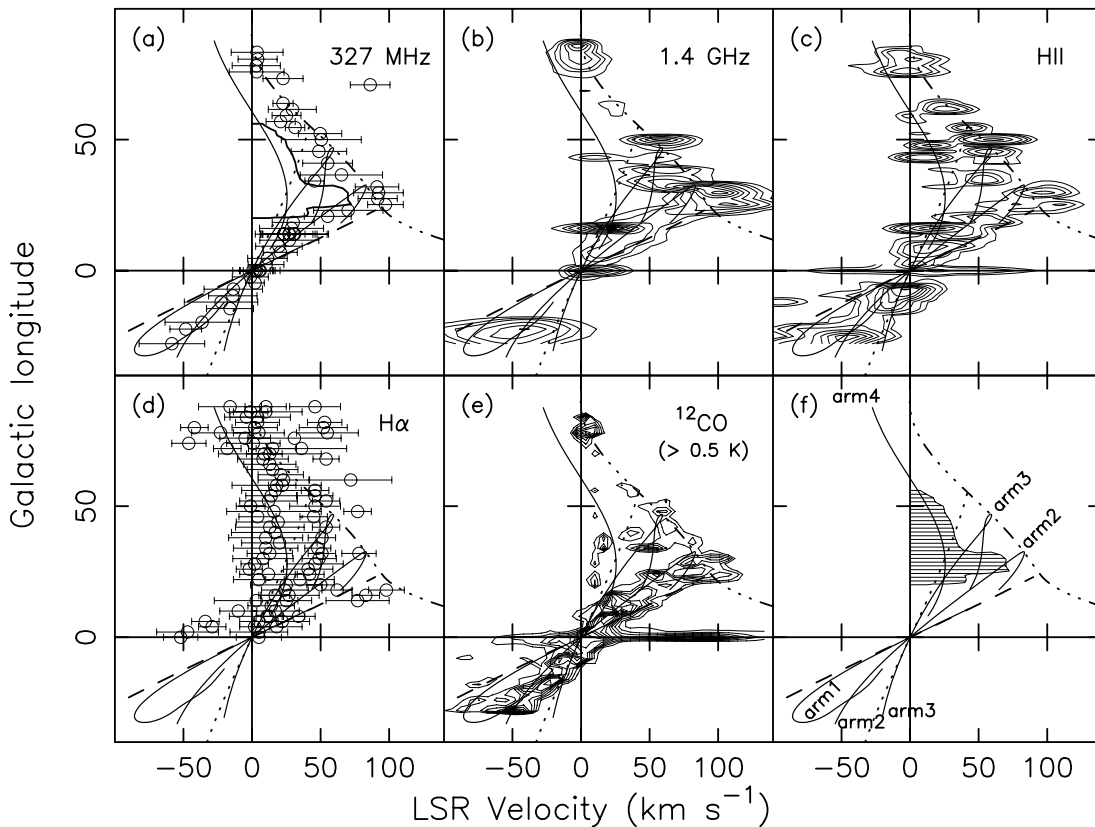
FIG. 5.—Longitude-velocity (l-v) diagram obtained from (a) hydrogen RRL emission at 327 MHz data, (b) composite spectra of hydrogen RRL emission near 1.4 GHz, (c) composite spectra of RRLs at 3 cm from H II regions, (d) Hα emission and (e) "intense" ^{12}CO emission. The l-v curves correspond to the four spiral arms (1–4 as designated by Taylor & Cordes 1993) are shown as solid lines in each of the l-v diagrams. For clarity, these curves are also shown separately in (f). The dashed and dotted lines in each frame correspond to gas at Galactocentric distances of 3.5 kpc and 7 kpc respectively. The dash-dot-dot-dot-dash line indicates the locus of tangent points. The striped region in (f) corresponds to a region devoid of line emission near 327 MHz. The boundary of this region is shown in (a). The contour levels in (b) are 10, 20, 30, 50, 70, 90, 110, 130, 150 mK; in (c) the levels are 10, 20, 30, 50 ,100, 150, 200, 250, 300, 400, 500, 600, 700 mK; and those in (d) are 0.5, 0.7, 0.9, 1.1, 1.3, 1.5, 1.7, 1.9, 2.1, 2.2 K. In (c), the contours for $l > 0°$ are made from the 3 cm RRL emission and those for $l < 0°$ are made from the 6 cm RRL emission from H II regions. The data are taken from Lockman (1976, 1980), Hart & Pedlar (1976), Cersosimo (1990), Heiles et al. (1996) (RRLs near 1.4 GHz), Downes et al. (1980), Caswell & Haynes (1987), Lockman (1989) (RRLs from H II regions), Reynolds (1983) (Hα), and Dame et al. (1987) (^{12}CO).

these lines. The emissions in the longitude range $l = 70°$–$85°$ correspond to the well-known Cygnus region which is abundant in thermal gas.

The striped area shown in Figure 5f shows a region in l-v space devoid of RRL emission near 327 MHz. This region can be mapped to an area in the Galactic disk by computing the near distances corresponding to the velocities bounding the shaded region. We have used the parameters of galactic rotation given by Burton & Gordon (1978) after scaling them to conform with $R_\odot = 8.5$ kpc and $\theta_0 = 220$ km s^{-1} for estimating the distances. Figure 6 shows this region in the Galactic disk, which is free of RRL emission at 327 MHz. The dots in Figure 6 represent H II regions of known distances in the longitude range $5°$–$90°$. The H II region data is taken from Georgelin & Georgelin (1976) and Downes et al. (1980). The kinematic distances given in the data are scaled by 0.85 to conform with $R_\odot = 8.5$ kpc. Figure 6 shows that the region devoid of RRL emission near 327 MHz is sparsely populated with H II regions. The absence of RRL emission at 327 MHz and known H II regions in this region of the Galactic disk may indicate that the low-density gas detected in this survey may be associated with known H II regions. The H II region data with distance certainty is however not complete in the longitude range $5°$–$90°$. In fact, the l-v diagram of high-frequency

RRLs from H II regions do show emission in the striped region of Figure 5f (Downes et al. 1980; Lockman 1989; Lockman et al. 1996). Thus there may be H II regions in the shaded region in Figure 6 which do not have any low-density gas associated with them. On the other hand the H II regions which occupy the striped region in Figure 5f can be at the "far" distance. Thus any low-density gas associated with them are not detected in RRL emission at 327 MHz either because of beam dilution or because of weaker background nonthermal emission, which reduces stimulated emission.

Similarities are seen in the l-v diagram shown in Figure 5a with that obtained by Anantharamaiah (1985a) using the H272α line detected with a beam of $2° \times 5.5$ toward selected sources in the longitude range $-2° < l < 50°$. The lower bound on the Galactocentric radius of ~ 3.5 kpc and the concentration of emission toward Galactocentric radius of ~ 5.0 kpc near the longitude $15°$ is evident in both the l-v diagrams. However, the extension of line emission to negative velocities in the longitude range $5° < l < 20°$ seen by Anantharamaiah (1985a) is not seen in the present observations. Furthermore, in the longitude range $20° < l < 40°$ Anantharamaiah (1985a) detected line emission over a larger velocity range (10 – 150 km s^{-1}) than in the present observations (40–120 km s^{-1}). These differences can be
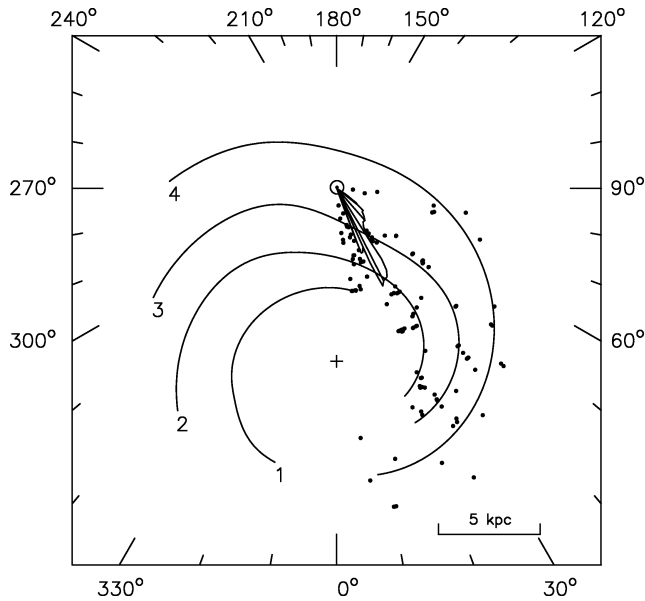
FIG. 6.—Four spiral arms of the galaxy as designated by Taylor & Cordes (1993). The H II regions with known distances in the longitude range 5°–90° are indicated by dots. The region in *l-v* space which is devoid of RRL emission near 327 MHz (see Fig. 5*f*) is mapped into physical space in the Galactic disk and shown as a jagged-edge region in the first quadrant near the Sun.

ascribed to the different beams used in the two observations. The present observations were made with a beam of ∼2° × 2°. Thus the nondetection of some of the emission features detected in the earlier observations with a beam of 2° × 5.5 could be because of beam dilution.

The association of the ionized gas producing RRL emission near 327 MHz with other components of the ISM in the Galactic disk can be studied by comparing the *l-v* diagram obtained for the tracers of the different components. The ionized components which are of present interest are: (1) the gas responsible for RRL emission near 1.4 GHz (Hart & Pedlar 1976; Lockman 1976, 1980; Cersosimo 1990; Heiles et al. 1996) which have been referred to as the ELDWIM (Petuchowski & Bennett 1993; Heiles 1994; Heiles et al. 1996); (2) normal H II regions which are prominent in radio continuum surveys (e.g. Altenhoff et al. 1978) and which are easily detected in higher frequency RRLs (e.g. Downes et al. 1980); and (3) the distributed ionized component referred to as the WIM. A good tracer of the WIM in the local ISM is the Hα emission (Reynolds 1983). Also of interest for comparison are the distribution of the molecular component of the ISM which is obtained using the ^{12}CO line and that of the atomic component obtained from the 21 cm H I emission. Here we compare the *l-v* diagram obtained for these different components with that from the present observations.

For the purpose of comparison of *l-v* diagrams, we have constructed composite spectra of different tracers by averaging the spectral emission within the 2° × 2°beam of our observations at different Galactic longitude. Figure 7 shows examples of composite spectra.

RRLs near 1.4 GHz have been observed at intervals of 1° in the Galactic plane by Lockman (1976, 1980) and Hart & Pedlar (1976) and more recently at finer intervals and also at higher Galactic latitudes by Heiles et al. (1996). Near

l = 335° RRLs were observed at this frequency by Cersosimo (1990). The HPBW of the observations of Lockman (1976, 1980) is 21′, that of Hart & Pedlar (1976) is 31′ × 33′, that of Heiles et al. (1996) is 36′(also 21′ for the observations with the 140 foot telescope), and that of Cersosimo (1990) is 34′. The composite spectra of RRL emission near 1.4 GHz were obtained from these data. Cersosimo (1990) and Lockman (1976,1980) have given the line intensity in antenna temperature. We have not attempted to convert them to brightness temperature for constructing the composite spectra. The *l-v* diagram made from the composite spectra near 1.4 GHz is shown in Figure 5*b*. No data near 1.4 GHz is available for the longitude range 340°–355°. Barring this longitude range, this *l-v* diagram is remarkably similar to that obtained from the 327 MHz observations (Fig. 5*a*). These similarities include (1) lack of emission at Galactocentric radius less than 3.5 kpc, (2) confinement of emission in the ∼5.0 kpc ring in the longitude range 5°–20°, (3) concentration of emission near the terminal velocity in the longitude range 50°–88° and (4) lack of emission in the shaded region between *l* = 20°–50° except near 40°. These similarities suggest that the RRL emission observed at 327 MHz and 1.4 GHz can be attributed to the same gas.

Figure 5*c* shows the *l-v* diagram of the composite spectra obtained from the RRL emission from H II regions. The data for this *l-v* diagram are taken from extensive RRL surveys of H II regions in the inner Galaxy made by Downes et al. (1980), Caswell & Haynes (1987), and Lockman (1989). In the longitude range 2° < *l* < 88° the most sensitive and fairly well-sampled survey was done by Lockman (1989) near 3 cm, and the composite spectra are obtained from this data. The composite spectra at longitudes *l* < 2° are obtained from the data of Downes et al. (1980) and Caswell & Haynes (1987). These observations were made near 6 cm. The RRL emission from the H II regions are observed at higher frequencies (>few GHz) and hence originate from higher density ionized gas. Near 327 MHz lines are not observed from such gas because of pressure broadening and large continuum opacity. The *l-v* diagrams obtained from these data can be similar if the low-density gas responsible for line emission near 327 MHz are associated with the H II regions. Although the *l-v* diagram of H II regions in Figure 5*c* in general shows some similarity with that obtained from 327 MHz observations, there are many differences. The similarities include (1) lack of emission at Galactocentric radius less than 3.5 kpc except near the Galactic center, and (2) concentration of emission near the terminal velocity in the longitude range 50°–88°. However, in general, H II regions seem to occupy a larger space in the *l-v* diagram. The H II regions show emission in the shaded region (shown in Fig. 5*f*) between *l* = 20°–50° and also a large velocity spread near *l* = 0°. The emission in the shaded region may be from H II region associated with arm 4 (see Fig. 6), which are at relatively large distances. Thus any low-density gas associated with these H II regions and which could produce line emission near 327 MHz may not be detected owing to large beam dilution and/or weak background continuum. In fact, the *l-v* diagram constructed from observations of RRLs near 327 MHz with a smaller beam of 2° × 5.5 do show some emission in the shaded region (Anantharamaiah 1985a).

The presence of a widely distributed WIM is evident from Hα (Reynolds 1983) and pulsar observations (Taylor & Cordes 1993). Information on the distribution of WIM in
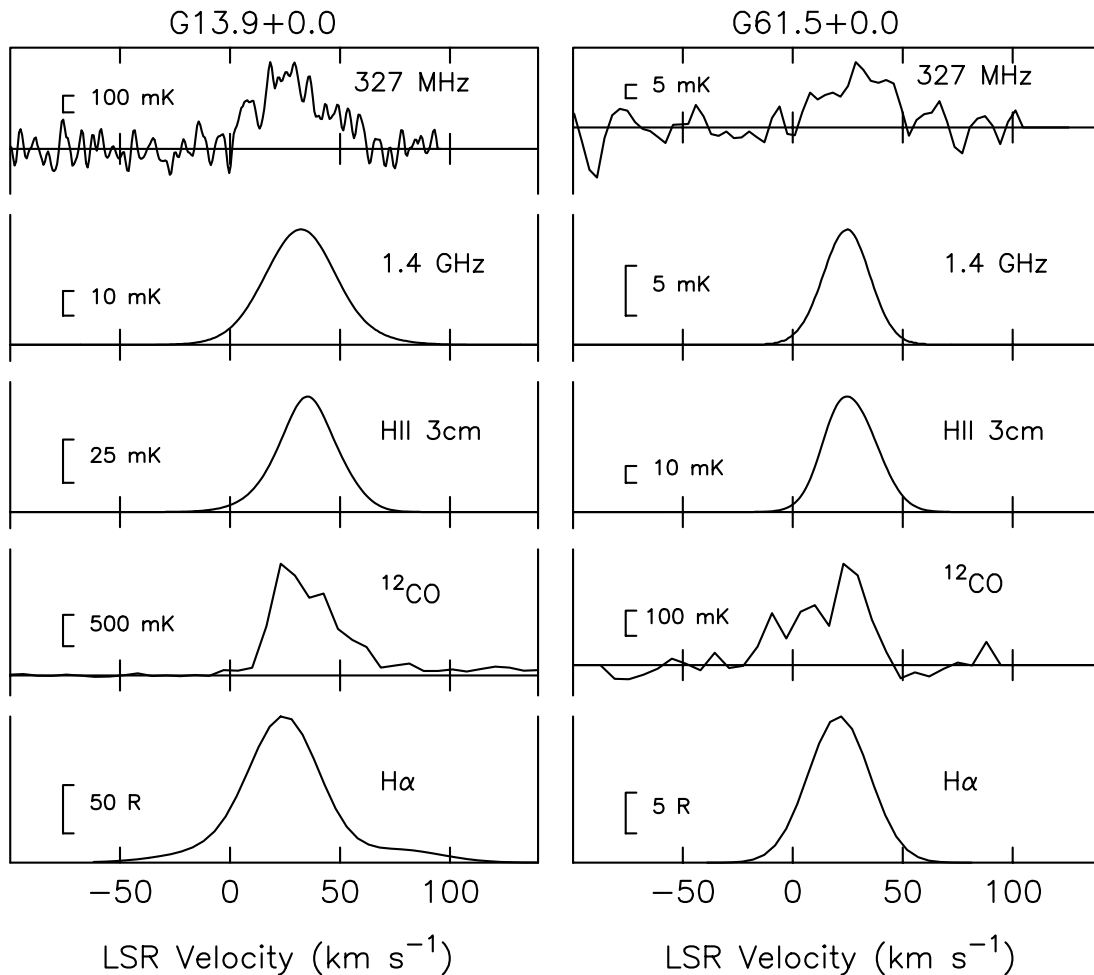
FIG. 7.—Composite spectra obtained from spectral tracers of different components of the ISM at two Galactic longitudes which are indicated at the top of the figure. The spectra from top to bottom are hydrogen recombination line near 327 MHz, H166α line near 1.4 GHz, RRL emission near 3 cm from H II regions, ^{12}CO line near 3 mm and the optical Hα line. The amplitude scale for each of the spectra is marked separately.

the Galactic plane from Hα observations are, however, limited owing to interstellar extinction. The typical mean free path of the Hα photons is about 1 kpc. Thus Hα observations largely probe ionized gas in the solar neighborhood even though these observations are far more sensitive than RRL observations. Nevertheless, comparison with the Hα observations is relevant to understand any possible association of RRL emission at 327 MHz with the WIM in the inner Galaxy. The distinct features of the Hα line profiles are multiple components and large "wings" (Reynolds 1983). On the other hand, the line profiles of RRLs near 327 MHz do not show any evidence, within the signal-to-noise ratio, of multiple components. Our observations are not sensitive to the "wings" of the profile owing to instrumental baseline uncertainties. In Figure 5d we have reproduced the l-v diagram given by Reynolds (1983) in the longitude range of interest. The Hα observations sample a field of diameter $0°.82$ spaced at 2° in longitude (Reynolds 1983). Figure 5d shows that, unlike RRL emission, Hα emission is present in almost all longitudes with LSR velocity ranging between 0 km s^{-1} and 60 km s^{-1}. The features detected in RRL observations beyond a velocity of 60 km s^{-1} are not seen in Hα because of large interstellar extinction (see below). Beyond $l = 50°$, the Hα emission also has components with veloci-

ties close to the terminal velocity at the corresponding longitude. It appears safe to conclude that the Hα emission observed by Reynolds (1983) and the RRLs observed near 327 MHz do not arise in the same gas.

The tracer of the molecular component of the ISM is the ^{12}CO emission. The composite spectra of ^{12}CO emission in the inner Galaxy were made from the data of Dame et al. (1987) and the l-v diagram obtained from their data is shown in Figure 5e. The velocity resolution of the composite spectra is smoothed to 6.5 km s^{-1} which is close to the typical final resolution of the data at 327 MHz. The lowest contour corresponds to an intensity level which is 25 times the typical RMS noise in the ^{12}CO spectra. These intense ^{12}CO emission corresponds to the "warm" molecular clouds discussed by Solomon, Sanders, & Rivolo (1985) and are associated with the star-forming region (see below for further discussion). The l-v diagram shown in Figure 5e is remarkably similar to that obtained from the present observations except the emission in the shaded region (shown in Figure 5f) and the large velocities of ^{12}CO emission near $l = 0°$. If the ^{12}CO emission in the shaded region corresponds to the "far" kinematic distance, then the RRL emission associated with them, if any, may not be detected for reasons stated earlier, like beam dilution and/or weak con-

tinuum background. Thus we conclude that the RRL emission near 327 MHz is associated with the star-forming regions.

The H I emission at any longitude extends over a large velocity range and is significantly different from the RRL emission near 327 MHz. This has been noted earlier by Lockman (1976) and Anantharamaiah (1985a).

4.3. Distribution of Low-Density Ionized Gas and Other Components in the Disk as a Function of R_{GC}

Although an l-v diagram gives a qualitative understanding of the distribution of ionized gas in the Galactic disk, a more quantitative study can be made by computing the average emission as a function of Galactocentric radius. Since the ionized gas at "near" and "far" kinematic distance will be at the same Galactocentric distance, the radial distribution is not affected by the two-fold ambiguity in estimating the line-of-sight distance. However the distribution will depend on the choice of the rotation curve.

The radial distribution is obtained as follows. The Galactic disk is subdivided into annuli at different Galactocentric radii. Consider an annulus of radius $R_{GC} = R_1$ and thickness ΔR (see Fig. 8). R_1 is less than $R_\odot$, the distance of the Sun from the Galactic center. In this case, all the lines of sight with longitudes less than $\sin^{-1}(R_{GC}/R_\odot)$ intersect the annulus at "near" and "far" distances. Near the tangent point, the two sections merge into a single one. The telescope, with a half power beam width of θ_B, receives radiation from ionized clouds situated at the two regions in the annulus. The spectral features produced by these clouds will be confined to a velocity range, say V_1–V_2, owing to differ-
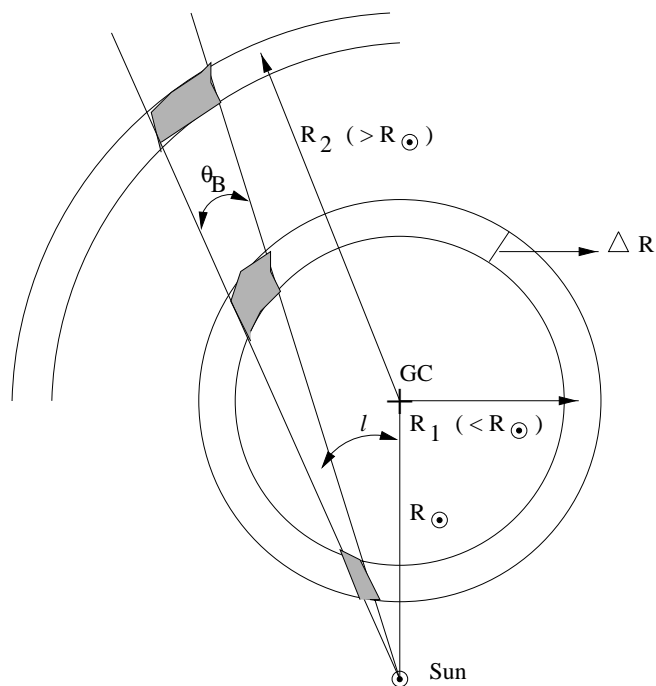

FIG. 8.—Geometrical representation of regions in an annular ring (*shaded areas*) in the Galactic plane that intersect a telescope beam of size θ_B pointed in the direction of Galactic longitude l. The annular ring has a thickness ΔR. Two cases are indicated. In the first case the ring is located inside the solar circle ($R_1 < R_\odot$) and in the second case the annular ring is outside the solar circle ($R_2 > R_\odot$). The two shaded regions of the inner ring have the same radial velocity.

ential galactic rotation. Given R_{GC}, ΔR, the beam width (FWHM) of the telescope and a galactic rotation curve, V_1 and V_2 can be computed. The average emission (Γ) in the annulus is then given by

$$\Gamma = \frac{\sum_{l1,l2} \int_{V_1}^{V_2} T_L \, dv}{A_R} \, . \qquad (1)$$

Here the summation of the integrated line intensity is over the longitude range $l1$–$l2$. The upper bound $|l2|$ is equal to $\sin^{-1}(R_{GC}/R_\odot)$ if $R_{GC} < R_\odot$ or limited by the longitude range of observation if $R_{GC} > R_\odot$. For longitudes close to $0°$, velocity crowding over long lines of sight makes the analysis very sensitive to the dispersion of the line profiles. Thus the computation is restricted to longitudes above a lower limit. We have used $|l_1| = 4°$ in our computation. A_R is the area of the annulus in the longitude range $l1$–$l2$ that contributes to the observed line emission. The telescope beam intersects only one region of the annulus for $R_{GC} > R_\odot$. The distribution function is obtained by computing the average emission as a function of R_{GC}. The spectral features beyond the terminal velocity at different longitudes are not included in the computation of average emission. Figure 9 shows the radial distribution obtained from the present data along with that obtained from the tracers of other components of the ISM. For the computation of all the radial distributions shown in Figure 9, the Galactocentric distance from 1.5 to 14 kpc was divided into annular rings of thickness 0.5 kpc. The average emission in each ring was then computed from the composite spectra of the different tracers as described above. The rotation curve used for the computation was taken from Burton & Gordon (1978) after scaling to $R_\odot = 8.5$ kpc and $\theta_0 = 220$ km s^{-1}. The computation of the distribution function was restricted to the longitude range $4° < l < 84°$, where the different components of the ISM are more or less uniformly sampled. The velocity range of the spectra observed near 327 MHz where carbon lines were present was eliminated to avoid its contribution to the average emission. In the case of H II regions, we have computed the average emission using the higher sensitivity RRL data near 3 cm by Lockman (1989). We also computed the surface density[2] of H II regions in the Galactic disk and is shown in Figure 9c. For this computation, the longitude range was divided into 1° bins and the data were taken from Lockman (1989) and Lockman et al. (1996). The distribution function shown in Figure 9f was obtained from spectral features in the ^{12}CO emission with intensity greater than 25 times the RMS noise in the spectra. The ^{12}CO data was taken from Dame et al. (1987) and the Hα data was from Reynolds (1983). The formal errors ($\pm 1 \, \sigma$) on the distribution for 327 MHz and ^{12}CO emission are also shown in the figure.

In the above calculation, it is implicitly assumed that the distribution of the ionized gas in the Galactic disk is axisymmetric. This means that the spiral arm structures in the Galactic disk are not considered for the radial distribution computation. A detailed analysis which include any association of line-emitting gas with the spiral arm structures will be presented elsewhere. We have also not corrected for the contribution to the line width due to intrinsic

---

[2] The surface density of H II regions are computed using the equation $\Gamma_s = [\sum_{l1,l2} \sum_{V_1} V_2 N(v, l)/A_R]$, where $N(v, l)$ is the number of H II regions in a unit LSR velocity interval.
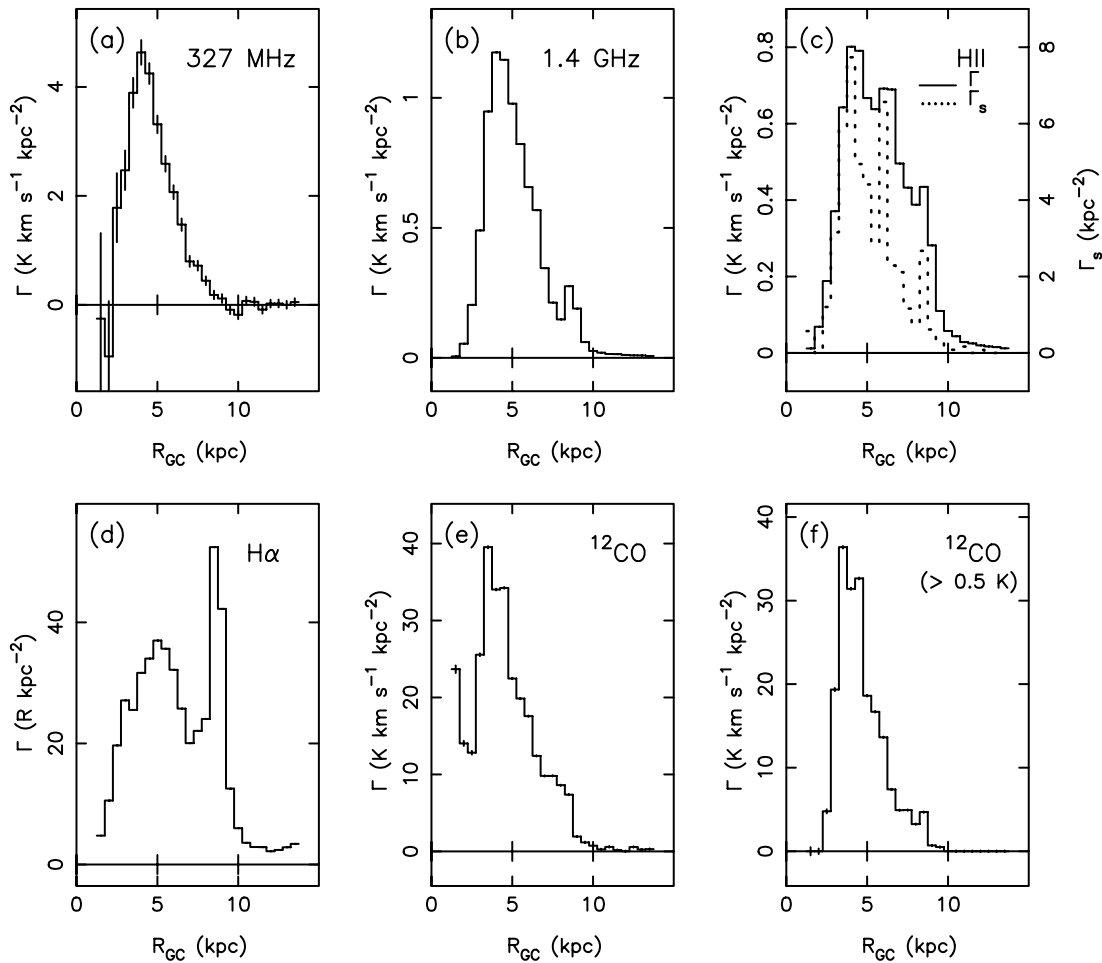
FIG. 9.—Plots of the radial distribution (average emission Γ vs. Galactocentric radius R_{GC}) of different components of the ISM. The radial distributions are obtained from (a) RRL emission from the Galactic plane near 327 MHz, (b) RRL emission from the plane near 1.4 GHz, (c) RRL emission from H II regions near 3 cm (solid line), (d) Hα emission in the Galactic plane, (e) ^{12}CO emission in the plane and (f) "intense" ($T_A > 0.5$ K) ^{12}CO emission from the Galactic plane. The radial distributions were computed using the data in the longitude range $4° < l < 84°$ where all the components of the ISM are well sampled. For computations using the 1.4 GHz and ^{12}CO data, we have used composite spectra obtained as explained in the text. The surface density (Γ_s) of H II regions as a function of Galactocentric radius is shown as dotted line in (c). The data are taken from Lockman (1976, 1980), Hart & Pedlar (1976), Cersosimo (1990), Heiles et al. (1996) (RRLs near 1.4 GHz), Lockman (1989), Lockman et al. (1996) (RRLs from H II regions), Reynolds (1983) (Hα), and Dame et al. (1987) (^{12}CO).

velocity dispersion, which will result in smearing of the true distribution. Furthermore, there is an overlap of the velocity interval computed using the galactic rotation model for different annuli at a given longitude. This is especially so near the terminal velocities at $l < 20°$. This overlap arises as a result of the large beam width of our observations. Because of this overlap in the velocity range, it is not possible to assign the line emission to a unique annulus. The net effect of this overlap is an overestimation of the average emission for Galactocentric distances less than 4 kpc. However, we found that the general shape of the distribution function is not significantly affected. Another factor that could affect the derived distribution is the effect of stimulated emission due to the galactic background radiation, which may favor detection of nearby clouds. This selection effect is not taken into account here.

The radial distribution obtained from the 327 MHz data (see Fig. 9a) shows that the average emission extends from $R_{GC} = 2.5$–9 kpc with a prominent peak near 4 kpc. Thus the distribution indicate that the RRLs detected in our observations do not originate in the solar neighborhood.

The distribution falls quite steeply on either side of the peak, the half power width being 3 kpc. The true distribution may be narrower than this because the broadening of the distribution due to intrinsic velocity dispersion has not been accounted for. Between 7 kpc and 8.5 kpc, the average emission is less than 20% of the peak, and it is near zero beyond 9 kpc. More than 70% of the RRL emission is confined between 2.5 kpc and 6 kpc. The concentration of power in RRL emission near 4 kpc was earlier pointed out by Lockman (1976) and Anantharamaiah (1985b). (The Galactic distance to Sun is taken as 10.0 kpc in these papers and hence the peak of the distribution quoted should be scaled by 0.85.) The distribution obtained by Anantharamaiah (1986) shows emission beyond 9 kpc. This emission should arise from gas at negative velocities in the longitude range $4°$–$84°$. In the present observations very little emission is observed at negative velocities in this longitude range. This behavior may be attributed to the difference in the angular resolutions of the observations.

The radial distribution obtained from RRL emission near 327 MHz is very similar to that obtained from the RRL

emission observed near 1.4 GHz (Fig. 9b). The peak of the distribution and the concentration of emission between 2.5 and 6 kpc are present in both Figures 9a and 9b. The excess emission seen near 8.5 kpc in the distribution of 1.4 GHz line emission is associated with the thermal gas near the Cygnus region. There is no corresponding excess emission seen in the distribution obtained from the present data. The line emission near 1.4 GHz from the Cygnus region may therefore have contribution from high-density H II regions, which are not detected in the observations near 327 MHz. The similarity of the l-v diagrams (Figs 5a and 5b) and the radial distributions of RRL emission in Figures 9a and 9b suggest that a considerable fraction of the line emission near 1.4 GHz originate from the same ionized gas that produces the line emission near 327 MHz.

The 3 cm RRL emission, which arises mostly in compact H II regions, has a broader radial distribution (see Fig. 9c) in the range $R_{GC} = 2.5–9$ kpc compared to the distribution obtained from the 327 MHz data. The distribution shows peaks near 4, 6 and 8.5 kpc, which corresponds to the spiral arm structures 2, 3 (as designated by Taylor & Cordes 1993) and the local Orion arm. The emission falls quite steeply for $R_{GC} < 4$ kpc, similar to that seen in the distribution of RRL emission near 327 MHz. We have also computed the surface density of H II regions and is shown in Figure 9c as a dotted line. For the computation of the surface density, both compact and diffuse H II region data are used. Although the surface density cannot be compared directly with the distributions obtained from line intensity, it has the advantage that RRL surveys of H II regions at different frequencies can be combined to obtain the radial distribution. The derived distribution is also not affected by the intrinsic velocity dispersion since only the central velocity is used for constructing the distribution. As expected, the surface density distribution is much narrower than the distribution of RRLs from the H II regions. The difference between the dashed and continuous curve in Figures 9c gives an indication of the maximum smearing that could occur as a result of line-width effects. Barring the peaks near 6 and 8.5 kpc, the surface density distribution looks very similar to the distribution obtained from the 327 MHz data.

The radial distribution obtained from the Hα observations (see Fig. 9d) shows that the emission is dominated by ionized gas close to Sun. This distribution is expected because the typical mean free path of the Hα photons is limited to about 1 kpc because of interstellar extinction. For this reason, the computed distribution shown in Figure 9d does not represent the true distribution of Hα emission in the Galactic disk. However it is significant that the average emission has not fallen to zero at $R_{GC} < 2$ kpc and the emission extends much beyond $R_{GC} = 9$ kpc. Thus the Hα emission is much more widespread in the inner Galaxy compared to RRL emission near 327 MHz.

Although the distribution of the molecular gas obtained from ^{12}CO emission (see Fig. 9e) also shows a peak near 4 kpc, there is a significant difference when compared to that of RRL emission near 327 MHz. For $R_{GC} < 2.5$ kpc the average emission does not fall to zero and, in fact, the total emission increases closer to the Galactic center. This increase has been discussed earlier by several authors (e.g. Combes 1991). However the distribution of the average emission of "intense" ^{12}CO emission shown in Figure 9f, shows good agreement with that of RRL emission. Solomon, Sanders, & Rivolo (1985) have found two classes

of molecular clouds in the Galactic disk—"warm" and "cold". The classification is based on the observed ^{12}CO line intensity. They have shown that the "warm" clouds (i.e., clouds with relatively intense ^{12}CO emission) form the spiral arm population and are associated with the H II regions. In obtaining the distribution in Figure 9f, we have used composite ^{12}CO spectra and the "intense" emission were obtained by using a threshold of 0.5 K. Thus, to first order these sites should be associated with the "warm" clouds and therefore to the sites of H II regions. We may thus conclude that the RRL emission obtained at 327 MHz in the Galactic disk is associated with star-forming regions.

The average emission of H I line, which samples the neutral component of the ISM, is more or less flat in the range 2.5 kpc $< R_{GC} < 8.5$ kpc and extends to distances greater than 14 kpc. Thus its distribution is distinctly different from the distribution of the RRL emission near 327 MHz, as has been noted earlier by Lockman (1976) and Anantharamaiah (1986).

4.4. Latitude Extent of RRL Emission

The spectra of RRL emission as a function of Galactic latitude at the two longitudes ($l = 0°.0$ and $13°.9$) are shown in Figures 1c and 1d. RRLs have been detected up to $±3°$ above the Galactic plane. The latitude extent of RRL emission at 1.4 GHz observed by Heiles et al. (1996) is similar to that seen in our observations. Figure 10 shows the observed line and continuum temperatures as a function of Galactic latitude. The FWHM of the latitude extent of RRL emission is $\sim 1°.8$. A scale height (FWHM) for the emission can be derived if the distance to the line-emitting region is known. At $l = 13°.9$, the "near" and "far" distances obtained from the measured central velocity is 3 and 13.5 kpc, respectively. The minimum scale height implied by the "near" distance is ~ 95 pc. Toward $l = 0°$, a kinematic distance to the cloud cannot be obtained. If we assume the distance to be halfway to the Galactic center, then the scale
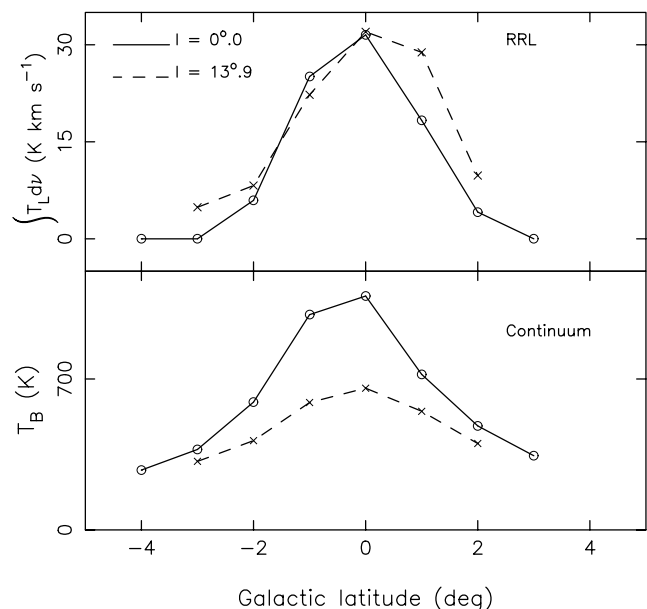

FIG. 10.—Variation of velocity-integrated recombination line intensity (top) and continuum brightness temperature (bottom) near 327 MHz as a function of Galactic latitude at two specific longitudes as indicated.

height turns out to be 133 pc. These values are close to that obtained for the molecular layer (~ 120 pc) and for the thermal gas that emits the 5 GHz continuum in the inner Galaxy (Combes 1991). The scale height of normal H II regions (~ 50 pc; Lockman et al. 1996) is about half that determined from line emission near 327 MHz.

Since, as shown in § 3.1.2, stimulated emission is the dominant mechanism for line emission near 327 MHz, the above determination of the scale height should be regarded as a lower limit. As the background continuum decreases with latitude, the sensitivity to line emission also decreases. In fact, if we use the line to continuum ratio, which partially corrects this effect, the FWHM of line emission comes out to be $\sim 3°$.

5. LINE EMISSION IN THE OUTER GALAXY

To compare with the inner Galaxy, we observed 14 positions in the outer Galaxy ($172° < l < 252°$). The angular resolution for these observations was also $\sim 2° \times 2°$. The coordinates of the observed positions are given in Table 1. The observed positions were equally spaced in longitude thus forming an unbiased sample. Five of the observed positions are devoid of any continuum source in the 2.7 GHz (Reich et al. 1990) and 408 MHz (Haslam et al. 1982) continuum surveys (see footnote b in Table 1). No RRLs were detected from these positions. Of the remaining nine positions, RRLs of hydrogen were marginally detected in three positions. The observed line parameters are given in Table 1. No carbon lines were detected. The hydrogen line detected at the position G207.08 + 0.00 may be associated with the Rosette nebula which has a similar radial velocity.

These observations show that the RRL emission near 327 MHz in the outer Galaxy is not as widespread as in the inner Galaxy. Since star formation activity is less in the outer galaxy, this result supports the conclusion of the earlier section that RRL emission near 327 MHz is associated with star forming regions. However, one selection effect that may have reduced the detection rate is the lower continuum background in the outer Galaxy.

6. SUMMARY AND CONCLUSION

This paper presents the results of a survey of RRLs near 327 MHz with an angular resolution of $\sim 2° \times 2°$. These observations are sensitive to low-density ($n_e \leq 50$ cm^{-3}) extended ionized gas in the Galactic plane. Hydrogen RRLs were detected in almost all directions in the inner Galaxy and carbon lines in several positions. In the outer Galaxy ($l = 172°–252°$), an unbiased set of 14 positions separated by $\sim 5°–7°$ were observed and lines were marginally

detected toward only three positions. These observations show that the line emission in the outer Galaxy is not as widespread as in the inner Galaxy. To study the latitude extent of the line emission in the inner Galaxy, we have observed RRLs as a function of Galactic latitude at two specific longitudes ($l = 0°0$ and $13°9$). RRLs were detected up to $b = \pm 3°$. We estimated that a lower limit to the scale height (FWHM) of line emission is ~ 100 pc.

The data is used to study the distribution of RRL emission in the Galactic disk by constructing l-v diagrams and also by computing the radial distribution of the ionized gas in the disk based on the observed velocities and a model of galactic rotation. The l-v diagram shows that most of the RRL emission originate from Galactocentric distance greater than 3.5 kpc. The line emission shows some confinement to the spiral arms at longitude less than 50°. The measured radial velocities of the RRLs in the longitude range 50°–90° are close to the terminal velocities at the corresponding longitudes. The radial distribution of RRL emission near 327 MHz shows a prominent peak near 4 kpc with 70% of the emission originating between Galactocentric radius 2.5 kpc and 6 kpc. The distribution falls steeply on either side of the peak.

The l-v diagram and the radial distribution obtained from the present data show good agreement with that obtained from RRL emission near 1.4 GHz, "intense" ^{12}CO emission and to some extent with the distribution of RRL emission from H II regions. On the other hand, the distribution of the Hα emission and H I emission in the Galactic disk is different from that of the RRL emission near 327 MHz. We conclude that the RRL emission at 327 MHz in the Galactic disk is associated with star forming regions. We also conclude that most of the RRL emission near 1.4 GHz originate from the same ionized gas that is responsible for line emission near 327 MHz.

REFERENCES

Altenhoff, W. J., Downes, D., Pauls, T., & Schraml, J. 1978, A&AS, 35, 23
Anantharamaiah, K. R. 1985a, J. Astrophys. Astron., 6, 177
———. 1985b, J. Astrophys. Astron., 6, 203
———. 1986, J. Astrophys. Astron., 7, 131
Burton, W. B. 1988, in Galactic and Extragalactic Radio Astronomy, ed. G. H. Verschuur & K. I. Kellermann (Berlin: Springer), 295
Burton, W. B., & Gordon, M. A. 1978, A&A, 63, 7
Caswell, J. L., & Haynes, R. F. 1987, A&A, 171, 261
Cersosimo, J. C. 1990, ApJ, 349, 67
Combes, F. 1991, ARA&A, 29, 195
Dame, T. M., et al. 1987, ApJ, 322, 706
Downes, D., Wilson, T. L., Bieging, J., & Wink, J. 1980, A&AS, 40, 379
Erickson, W. C., McConnell, D., & Anantharamaiah, K. R. 1995, ApJ, 454, 125
Georgelin, Y. M., & Georgelin, Y. P. 1976, A&A, 49, 57
Gordon, M. A., & Cato, T. 1972, ApJ, 176, 587
Gottesman, S. T., & Gordon M. A. 1970, ApJ, 162, L93

Hart, L., & Pedlar, A. 1976, MNRAS, 176, 547
Haslam, C. G. T., Salter, C. J., Stoffel, H., & Wilson, W. E. 1982, A&AS, 47, 1
Heiles, C. 1994, ApJ, 436, 720
Heiles, C., Reach, W. T., & Koo, B.-C. 1996, ApJ, 466, 191
Kerr, F. J., & Lynden-Bell D. 1986, MNRAS, 221, 1023
Konovalenko, A. A., & Sodin, L. G. 1980, Nature, 283, 360
Kulkarni, S. R., & Heiles C. 1988, in Galactic and Extragalactic Radio Astronomy, ed. G. H. Verschuur & K. I. (Berlin: Springer), 95
Lockman, F. J. 1976, ApJ, 209, 42
Lockman, F. J. 1980, in Radio Recombination Lines, ed. P. A. Shaver (Dordrecht: Reidel), 185
———. 1989, ApJS, 71, 469
Lockman, F., J., Pisano, D., J., & Howards, G., J. 1996, ApJ, 472, 173
Matthews, H. E., Pedlar, A., & Davies, R. D. 1973, MNRAS, 165, 149
McKee, C. F., & Ostriker, J. P. 1977, ApJ, 196, 565
Mezger, P. G. 1978, A&A, 70, 565

Payne, H. E., Anantharamaiah, K. R., & Erickson, W. C. 1989, ApJ, 341, 890

Petuchowski, S. J., & Bennett, C. L. 1993, ApJ, 405, 591

Pedlar, A., Davies, R. D., Hart, L., & Shaver, P. A. 1978, MNRAS, 182, 473

Reich, W., Fürst, E., Reich, P., & Reif, K. 1990, A&AS, 85, 633

Reynolds, R. J. 1990, in IAU Symp. 139, The Galactic and Extragalactic Background Radiation, ed. S. Bowyer & C. Leinart (Dordrecht: Kluwer), 157

———. 1983, ApJ, 268, 698

Roshi, D. A., & Anantharamaiah, K. R. 1997, MNRAS, 292, 63

Salter, C. J., Maddalena, R. J., & Garwood, B. 1994, Unipops CookBook, NRAO

Shaver, P. A. 1975, Pramana, 5, 1

———. 1976, A&A, 49, 1

Shaver, P. A., McGee, R. X., & Pottasch, S. R. 1979, Nature, 280, 476

Solomon, P. M., Sanders, D. B., & Rivolo, A. R. 1985, ApJ, 292, L19

Subrahmanyan R. 1989, Ph.D. thesis, Indian Institute of Science

Swarup, G., et al. 1971, Nature, 230, 185

Taylor, J. H., & Cordes, J., M. 1993, ApJ, 411, 674

Wood, D. O. S., & Churchwell, E. 1989, ApJS, 69, 831